Three-material decomposition with spectral CT to assess bone mineral density for the early diagnosis of osteoporosis

Writing assignment

MSc Medical Imaging

Sara Guillén Fernández-Micheltorena

Examination committee:

Supervisor: dr. ir. Koen Vincken

Assistant professor, UMC Utrecht

Reviewer: dr. Wouter Foppen

Radiologist, UMC Utrecht

Utrecht, 25th September 2023

Three-material decomposition with spectral CT to assess bone mineral density for the early diagnosis of osteoporosis

Sara Guillén Fernández-Micheltorena
Utrecht University

***Abstract*—Osteoporosis, a prevalent skeletal disorder affecting postmenopausal women and older adults, leads to reduced bone mass and deteriorating bone microarchitecture, resulting in heightened fracture risk. Early diagnosis is crucial for timely treatment and fracture prevention. Bone mineral density (BMD) estimation is pivotal in this regard, with trabecular tissue providing key insights. Dual-Energy X-ray Absorptiometry (DXA) and Quantitative Computed Tomography (QCT) are the current clinical standards but come with several limitations. Spectral CT, a promising technology, overcomes these limitations by employing dual-energy techniques. It quantifies materials based on distinct attenuation properties at different energy levels. A three-material decomposition technique shows potential in dual-energy CT, enabling BMD quantification without a calibration phantom and addressing adipose tissue influence. This review explores the application of three-material decomposition in spectral CT for osteoporosis BMD assessment, evaluating existing techniques, strengths, and limitations, and offering insights into spectral CT's potential in early diagnosis and osteoporosis management, outlining future directions, including technological advancements and improved BMD analysis using three-material decomposition in spectral CT.**

***Index Terms*—osteoporosis, spectral CT, three-material decomposition**

1. Introduction

Osteoporosis is a prevalent skeletal disorder that affects millions of individuals worldwide, particularly postmenopausal women and older adults [1]. It is characterized by reduced bone mass and deterioration of bone microarchitecture, leading to increased bone fragility and a heightened risk of fractures [2]. The World Health Organization (WHO) estimates that worldwide, one in three women over the age of 50 will experience osteoporotic fractures, along with one in five men in the same age group [3]. These fractures can have severe consequences, including pain, disability, reduced quality of life, and increased mortality rates [4].

Early diagnosis of osteoporosis is paramount to avoid the development of fractures and begin early treatment to deter further bone mass decline. To detect early signs of osteoporosis, bone mineral density (BMD) must be estimated. The BMD is representative of the presence, and in what quantity, of minerals such as calcium hydroxyapatite (HA) within the bone and it is best observed on the trabecular tissue [5].

The current gold standard technique for BMD assessment is Dual-Energy X-ray Absorptiometry (DXA) [6]. DXA is a non-invasive technique characterized by its low radiation exposure and cost-effectiveness [7]. However, its two-dimensional nature makes it size-dependent [8]. Furthermore, DXA is unable to differentiate between compact cortical bone and porous trabecular bone [8]. Quantitative Computed Tomography (QCT) is a widely used method for assessing BMD volumetrically. Contrary to DXA, QCT measurements are independent of body size and provide the ability to separately analyze cortical and trabecular bone [9]. However, it's important to note that QCT involves higher radiation exposure and requires the use of a phantom for calibration. Additionally, the impact of adipose tissue in bone marrow on QCT measurements has been investigated in several studies, revealing a tendency for BMD underestimation [10].

Spectral CT imaging has emerged as a promising technology with the potential to address the limitations of conventional CT and offer additional advantages for BMD assessment [11]. Dual-energy spectral CT offers increased information acquisition by capturing attenuation values at two distinct energy levels. This feature permits the differentiation and quantification of materials with varying attenuation properties at specific energies. The majority of dual-energy CT (DECT) acquisition methods, such as rapid kVp switching and dual-source CT, necessitate prospective techniques entailing specific acquisition protocols [12]. A more recent advancement is the dual-layer detector CT (DLCT) system, which inherently captures dual-layer energy information, eliminating the necessity for dedicated acquisition protocols, with lower radiation exposure and the potential for opportunistic screening [13].

Previous works have highlighted the potential of employing a three-material decomposition technique for BMD assessment in DECT images [14]. This same approach has also demonstrated efficacy in distinguishing between acute and chronic thoracolumbar vertebral fractures based on the extent of bone marrow edema [15]. Consequently, the implementation of a three-material decomposition method holds the potential for enabling BMD quantification without the need for a calibration phantom, while simultaneously mitigating the effect of adipose tissue.

The purpose of this literature review is to investigate the use of spectral CT with the three-material decomposition approach for assessing BMD in the diagnosis of osteoporosis. The existing methods for assessing BMD, along with their respective advantages and limitations, are addressed in Section 2. The

fundamental principles and technological progress of spectral CT are explained in Section 3. The progression towards three-material decomposition and recent advancements are discussed in Section 4. The challenges encountered and potential future directions in this field are proposed in Section 5, culminating in a conclusion in Section 6.

2. Osteoporosis and bone mineral density

2.1. Definition of osteoporosis

Osteoporosis, the most prevalent metabolic bone disease worldwide, has emerged as a significant public health concern and economic burden [16]. This condition is characterized by the progressive loss of bone mass and deterioration of bone microarchitecture, both of which contribute to an increased risk of skeletal fragility and fractures [2]. Fragility or low-trauma fractures are the main sources of morbidity and mortality associated with osteoporosis. Thus, the primary objective of managing osteoporosis is the prevention of these fractures [17].

Early diagnosis plays a crucial role in the effective management of osteoporosis. Unfortunately, clinical detection of osteoporosis is often challenging before a fracture event occurs [17]. By identifying bone loss at an early stage, further disease progression and subsequent fractures can be mitigated.

Osteoporosis is associated with an imbalance in bone remodeling, in which there is relatively greater bone resorption than bone formation. The principal consequence of bone structure is that trabecular bone (the spongy inner part of bones) loses its density.

Consequently, trabecular bone (the spongy inner part of bones) loses its density and cortical bone (the outer shell) thins [18] (see Fig. **??**. This structural deterioration weakens the bones, making them more susceptible to fractures even with minimal trauma or stress. Sites that have high trabecular bone content (posterior–anterior spine) are more metabolically active; therefore, a significant change in BMD is likely to occur earlier at the spine than at the hip or forearm [19].

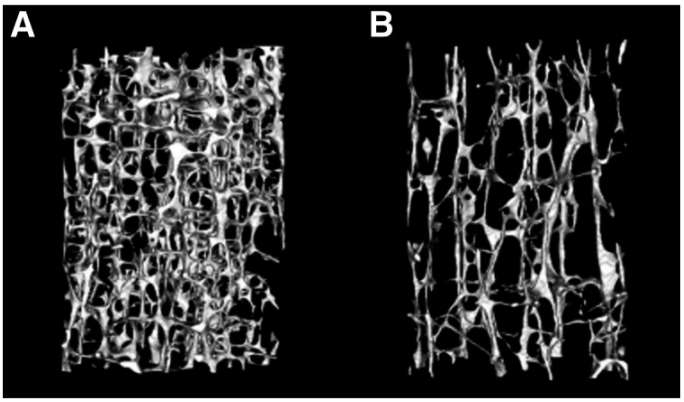

Fig. 1: Three-dimensional micro-CT where the loss of BMD in trabecular bone in osteoporosis can be observed for a 52-year-old woman (A) and 84-year-old woman (B) with vertebral fracture. Source: [6]

Osteoporosis predominantly affects older adults, especially women post-menopause, due to the decline in estrogen levels [20]. Individuals with a family history of osteoporosis, a personal history of fractures, or certain medical conditions like hyperthyroidism, rheumatoid arthritis, or gastrointestinal disorders are also at higher risk [21]. Sedentary individuals, those with low calcium and vitamin D intake, smokers, heavy alcohol consumers, and those with low body weight are prone to osteoporosis [21].

2.2. Diagosis of osteoporosis

The most commonly utilized method for identifying osteoporosis and assessing bone health is through the measurement of BMD, a process called bone densitometry. Bone mineral density can be defined as the amount of bone mass per unit volume (volumetric density, g/cm^3), or per unit area (areal density, g/cm^2). The standard techniques for BMD assessment are DXA and QCT.

2.2.1. DXA

DXA stands as the cornerstone of bone densitometry, representing a well-established clinical approach for assessing BMD based on a 2-D projectional area measurement (aBMD). Employed as both an initial screening tool and a follow-up mechanism, DXA offers a means to appraise the effectiveness of therapeutic interventions for osteopenia (low bone mass) and osteoporosis. The precision and consistency exhibited by DXA measurements have paved the way for the formulation of diagnostic criteria for osteoporosis, as outlined by the WHO [22].

This technique is non-invasive and works by passing two X-ray beams of different energy levels through the bones. It is characterized by its cost-effectiveness and low radiation exposure. However, it also has some limitations. Firstly, the two-dimensional nature of this method makes the BMD measurement susceptible to overlying structures and degenerative bone changes that artificially increase the BMD values [8]. DXA measurements are also dependent on body size as it determines the areal BMD. Therefore, BMD measurements can be underestimated in small patients and overestimated in tall patients [8]. Moreover, DXA is unable to differentiate between compact cortical bone and porous trabecular bone [8].

The diagnosis relies on T-scores, which indicate how many standard deviations above or below the average BMD of a reference population the patient's BMD falls. These T-scores are influenced by gender and race. The WHO classifies normal BMD as having a T-scores exceeding –1.0. Low bone mass or osteopenia is characterized by t-scores ranging from –1.0 to –2.4, while T-scores of –2.5 or lower indicate the presence of osteoporosis. [11].

2.2.2. QCT

QCT provides volumetric BMD (vBMD), and both the trabecular and cortical bone compartments can be assessed [23]. It presents several advantages over DXA due to its three-dimensional nature and its ability to leverage routine CT scans.

A key disparity between these two technologies pertains to the tracking of bone density changes. QCT-measured spine BMD values tend to exhibit relatively accelerated rates of bone loss with advancing age when contrasted with DXA values [24]. This difference is primarily attributed to QCT's focus on trabecular bone measurements, where the rate of change is more pronounced compared to cortical bone [9].

Nevertheless, the practical use of QCT for frequent or longitudinal BMD assessments is limited by the higher radiation exposure required in comparison to DXA scans [7]. Additionally, the influence of adipose tissue in bone marrow on QCT measurements has been the subject of investigation in several studies, revealing a tendency for BMD underestimation [25]. Furthermore, proper positioning of a bone density calibration (BDC) phantom within the scanner, a step that can occasionally be overlooked, is crucial for accurate QCT measurements.

It's important to recognize that the WHO-defined spine T-scores for osteoporosis, derived from DXA data, are not directly applicable to QCT. The American College of Radiology provides threshold values following the World Health Organization (WHO) DXA guidelines, as there are presently no established WHO diagnostic guidelines specific to QCT. According to these guidelines, osteoporosis is identified when the BMD in the spine falls below 80 mg/cm^3 HA, osteopenia is categorized for BMD ranging between 80 and 120 mg/cm^3 HA, while BMD measurements surpassing 120 mg/cm^3 HA are classified as normal [26]. The two classification criteria for DXA and QCT are shown in Table I.

TABLE I: Classification of osteoporosis for QCT and DXA

Classification	**QCT (mg/cm^3)**	**DXA (T-score)**
Normal	$>$ 120	$>$ -1.0
Ostopenia	$>$ 80, $<$ 120	$>$ -1.0, $<$ -2.5
Osteoporosis	$<$ 80	$<$ -2.5

In practice, DXA typically serves as the primary tool for initial screening and follow-up in bone density assessment, while QCT is utilized as a complementary technique. Cases, where QCT offers advantages over DXA, include situations involving extreme variations in body height (very large and very small patients), instances of significant spinal degenerative disease, severely obese patients, and scenarios requiring heightened sensitivity to subtle changes in trabecular bone density [26].

3. Spectral CT Imaging

The diagnosis and evaluation of osteoporosis have long relied on established techniques such as DXA and QCT. However, the evolving landscape of technology has ushered in a new era with the advent of spectral CT, also known as DECT. This innovative approach harnesses the power of dual X-ray energy levels, offering a more nuanced understanding of scanned tissues compared to traditional methods. The allure of spectral CT lies in its potential to address the limitations of existing standards, propelling it into the forefront of medical imaging advancements.

3.1. Physical basis

Conventional X-rays have long been the foundation for assessing how materials interact with radiation. Two primary interactions, the photoelectric effect and Compton scattering, play essential roles in how X-rays and matter interplay, affecting image contrast and overall attenuation. The linear attenuation coefficient (μ) quantifies the proportion of X-ray beam attenuation per unit thickness of the attenuating material. It is influenced by factors such as the energy of the X-ray beam (E), the atomic number (Z), and the physical density (ρ) of the material [27]. In the context of CT, the μ value for each scanned voxel (represented as r, the specific unit volume) can be obtained from the CT Hounsfield unit (HU) value:

$$\mu(E) = \frac{HU(E) * \mu_{water}(E)}{1000[HU]} + \mu_{water}(E) \qquad (1)$$

The HU is a standardized scale based on the linear attenuation coefficient of the tissue contained within the voxel, relative to that of water.

The linear attenuation coefficient μ can be considered approximately proportional to the physical density, being μ/ρ the mass attenuation coefficient [28].

In traditional CT, a single X-ray beam energy is used, leading to a loss of energy dependence in tissues. Consequently, tissues with similar attenuation coefficients obtain identical HU values when exposed to the same X-ray beam energy. This similarity hinders differentiation between these tissues. An example is calcium and iodine, which may have the same attenuation at different densities (concentrations) and thus will have the same HU value. However, they present different attenuation curves (linear attenuation coefficients as a function of energy) and if scanned at different energies, they can be differentiated (see Fig. 2).

This is why spectral CT was introduced, as it capitalizes the energy dependence of tissues offering a superior material differentiation. This aspect holds particular significance in the context of osteoporosis, especially when evaluating BMD. Conventional CT measurements of BMD often exhibit underestimation due to the intricate composition of bone tissue. By enabling precise material differentiation, spectral CT enables more precise quantification, thereby offering the potential for more accurate assessments.

The specific material decomposition techniques employed for material differentiation and quantification are discussed in Section 4.

3.2. Technology

The commonly used technique is dual-energy spectral CT which employs two distinct X-ray energy spectra for the imaging process, one high energy and one low energy.

In the 1980s, various research groups investigated DECT's potential for BMD assessment, enabling measurements with minimal interference from bone marrow fat [11], [30]–[33].

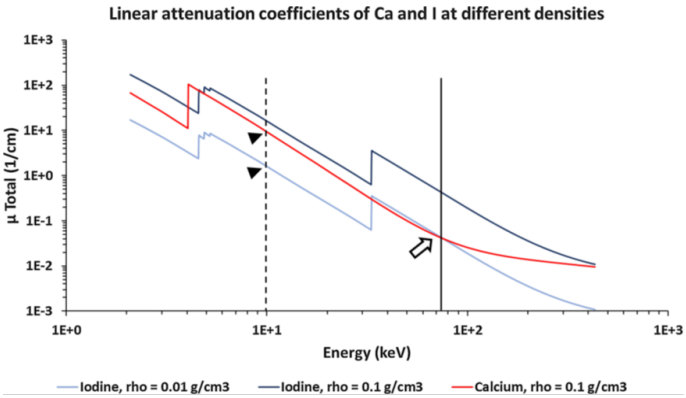

Fig. 2: This graph shows the linear attenuation coefficient of iodine at two different densities and calcium as a function of the energy of the incident X-ray photon. If iodine at $0.01 g/cm^3$ and calcium are irradiated with an energy of $\approx$ 75keV (black solid line), both will show the same HU value. However, if irradiated with an energy of 10 keV (black dashed line), the materials can be distinguished. Source: [29].

However, limitations such as increased radiation dosage associated with DECT and the enhanced precision offered by single-energy CT protocols led to the temporary abandonment of DECT. A decade ago, the landscape shifted, resulting in a resurgence of interest in DECT, which culminated in its commercial availability [14], [34]–[36]. Since then, BMD has been evaluated with dual source DECT (dsDECT) [14], [34], [35] and rapid kVp switching DECT [36].

In dsDECT scanners, there are two separate X-ray tubes and two distinct detectors integrated, each positioned within the gantry at an approximate 90º offset from the other. In the case of fast kVp switching scanners, the X-ray tube switches back and forth between low and high energy during the same rotation, capturing both sets of projections. However, these advanced technologies require specialized examination protocols, can be susceptible to motion artifacts, and are linked to elevated radiation exposure [12].

A recent innovation in DECT technology, the dual-layer detector CT (DLCT) has been introduced. This pioneering technique consists of a single tube that gives a polychromatic X-ray beam (120 or 140 kVp) and a dual-layer detector that performs the spectral separation. The layer detector is composed of two layers: the inner one is sensitive to low energies and the external one, to high energies. A standard clinical image is reconstructed from the data of both layers without the requirement of preselecting a DECT protocol [37]. Furthermore, compared to the other methods, it does not expose the patient to higher radiation doses [38].

Another significant benefit of DLCT systems is that the dual-energy information from these layers is accessible in every standard clinical examination. This stands in contrast to dual-source or rapid kV-switching systems, where the acquisition of dual-energy information takes place only upon prior prescription before the examination. As a result, DLCT offers an ongoing potential for additional analyses using previously acquired imaging data, such as BMD measurements in scans not explicitly intended for this purpose. This potential could potentially eliminate the requirement for an additional DXA scan [13].

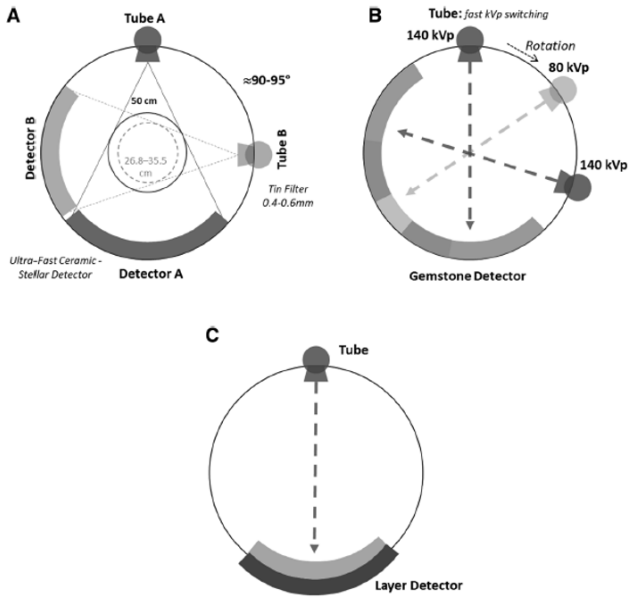

Fig. 3: Drawing of the 3 mentioned DECT systems. A) Dual-source DECT with two sources and two detectors placed at approximately 90º. B) Rapid kVp switching DECT. C) Dual-layer DECT with one detector with two layers for low and high energies. Source: [29]

4. Three-material decomposition of Spectral CT Data

Once information is acquired from the DECT system, material decomposition is employed to measure the materials within an image by utilizing their unique attenuation characteristics at various energy levels. While many studies have predominantly employed the two-material decomposition approach due to its straightforward nature, recently, three-material decomposition algorithms have been developed and put into practice, offering enhanced accuracy in material differentiation.

4.1. Two-material decomposition

The first two-basis-material decomposition algorithm was developed by Alvarez and Macovski [39]. The principle behind this algorithm is that the interaction of X-rays in any material can be roughly approximated as a linear combination of each attenuation phenomenon or the relative mass attenuation coefficients of each phenomenon, being the most relevant the photoelectric effect (μ_P/ρ) and Compton scattering (μ_C/ρ):

$$\frac{\mu}{\rho}(E) \approx \frac{\mu_P}{\rho}(E) + \frac{\mu_C}{\rho}(E) \tag{2}$$

where $\frac{\mu}{\rho}$ is the mass attenuation coefficient of a material at energy E.

This demonstrates that with a conventional X-ray beam, the effective attenuation coefficient can be computed by factoring in the contributions of Compton and photoelectric interactions, which are modeled based on the effective density (ρ_{eff}). From Eq. 2:

$$\mu_{eff} \approx \rho_{eff} \left(\frac{\mu_P}{\rho}(E) + \frac{\mu_C}{\rho}(E) \right) \tag{3}$$

From the work of Alvarez and Macovski, Kalender et al. defined the mass attenuation coefficient of a given mixture, as a function of energy, with a linear combination of the mass attenuation coefficients of two hypothetical known basis materials (1 and 2) present at different mass densities (ρ_1 and ρ_2) at a given position r [40]:

$$\mu(r, E) = \rho_1(r) \left(\frac{\mu}{\rho} \right)_1 (E) + \rho_2(r) \left(\frac{\mu}{\rho} \right)_2 (E) \tag{4}$$

The linear attenuation coefficient at a specific spatial location, $\mu(r, E)$ (representing the measured attenuation in CT), results from the combination of two distinct materials with known mass attenuation coefficients $(\mu/\rho)_{1,2}(E)$, each existing at unknown mass densities within the voxel (denoted as ρ_1 and ρ_2). It's important to note there is no solution to this equation when a single X-ray spectrum is employed [40].

If we measure the attenuation coefficients after irradiation with two X-ray energies (high and low, $E_{H,L}$), Eq. 4 can be solved as a system of two equations with two unknowns (ρ_1 and ρ_2).

$$\begin{cases} \mu(r, E_H) = \rho_1(r) \left(\frac{\mu}{\rho} \right)_1 (E_H) + \rho_2(r) \left(\frac{\mu}{\rho} \right)_2 (E_H)) \\ \mu(r, E_L) = \rho_1(r) \left(\frac{\mu}{\rho} \right)_1 (E_L) + \rho_2(r) \left(\frac{\mu}{\rho} \right)_2 (E_L)) \end{cases} \tag{5}$$

Applying this algorithm allows, material-selective images can be obtained where the basis materials (e.g., calcium and iodine) are detected, labeled, quantified, displayed, or subtracted [33]. Some examples of material-specific images are iodine maps or virtual non-contrast images.

After computing the effective densities of the fundamental materials (ρ_1 and ρ_2), the linear attenuation coefficient of the mixture ($\mu(r, E)$) and consequently the CT numbers can be determined by simulating irradiation with a virtual monochromatic beam spanning a wide range of energies, including those beyond the effective energy range. These resulting images are referred to as virtual monoenergetic images (VMI) (see Fig. 4). VMI obtained at lower keV values prove beneficial for enhancing focal lesions with low contrast. They can also contribute to improving the contrast-to-noise ratio and reducing the need for administered contrast agents [41]. Conversely, VMI obtained at higher keV values are valuable for mitigating issues like proton-starving and beam-hardening artifacts that arise in the presence of metallic objects. This advantage, however, comes at the cost of reduced contrast [42]. A disadvantage when using VMI algorithms is that noise increases with lower energies which has already been addressed with noise-reduction systems [43].

4.2. Three-material decomposition

In principle, dual-energy CT scans can characterize an object with up to two constituent elements as they offer only two independent measurements. However, there exist three-material decomposition algorithms that can leverage two datasets to obtain the fractions of three distinct materials.

The most straightforward approach is provided by Goodsitt et al. [30]. The authors began with the assumption that the effective linear attenuation coefficient as a function of X-ray energy, $\mu_{eff}(E)$, is derived from the summation of the mass attenuation coefficients of each basis material (i) multiplied by their respective concentrations. Here, the concentration c_i is defined as the product of the fractional volume V_i and mass density (ρ_i).

$$\mu_{eff} = \sum_i \frac{\mu_i(E)}{\rho_i} c_i \tag{6}$$

Substituting Eq. 1 in Eq. 6 and given that the conservation of volume is respected, a system of three equations can be solved (Eq. 7):

$$\begin{cases} CT(E_H) = V_1 CT_1(E_H) + V_2 CT_2(E_H) + V_3 CT_3(E_H) \\ CT(E_L) = V_1 CT_1(E_L) + V_2 CT_2(E_L) + V_3 CT_3(E_L) \\ V_1 + V_2 + V_3 \approx 1 \end{cases} \tag{7}$$

This model allows the computation, within the image domain, of the fractional volumes ($V_{1,2,3}$) of three fundamental materials, through two measurements, while adhering to a third criterion (the preservation of volume). However, the attenuation in the image can be affected by noise and thus, the sum of the fractional volumes can not always considered to be exactly 1. Therefore, the algorithms that implement this method add constraints such as making the sum equal or greater than 95 ($V_1 + V_2 + V_3 \geq 0.95$) [44]. Additionally, the applicability of this model is limited by instances where volume conservation is not maintained universally (e.g., salt in water or iron in fat or soft tissue).

A more generalized model was proposed in [45], based on the conservation of mass. In the first step of the model, the dual-energy datasets are used to calculate the $\rho_{eff}(E)$. In the second step, the $\rho_{eff}(E)$ is used in a system of three equations (Eq. 8) where the fractional masses ($f_{1,2,3}$) of the three materials are the unknowns and the conservation of mass is respected:

$$\begin{cases} \mu_{eff,L} = \rho_{eff}(\mu_{m1}(E_L) * f_1 + \mu_{m2}(E_L) * f_2 + \mu_{m3}(E_L) * f_3) \\ \mu_{eff,H} = \rho_{eff}(\mu_{m1}(E_H) * f_1 + \mu_{m2}(E_H) * f_2 + \mu_{m3}(E_H) * f_3) \\ f_1 + f_2 + f_3 = 1 \end{cases} \tag{8}$$

By solving the linear equation system on a pixel-by-pixel base for f_1, f_2, and f_3, 3D images for all material volume fractions are generated.

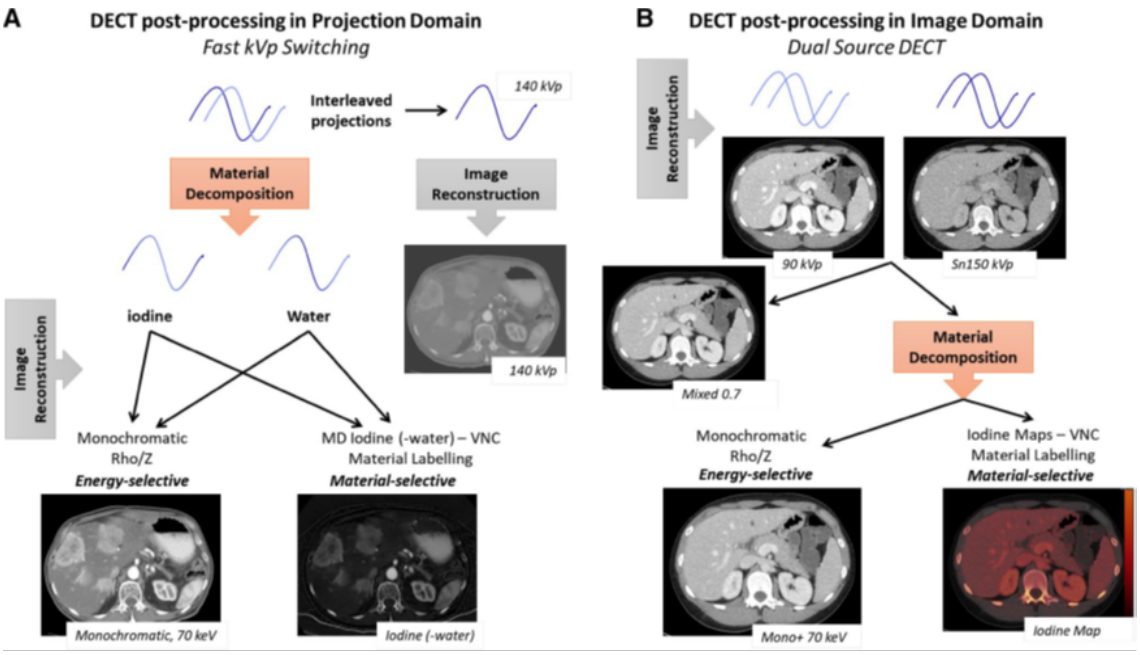

Fig. 4: Post-processing step in DECT data. A) Example of material decomposition in projection domain using a fast kVp switching system to obtain energy-selective (VMI) and material-selective (iodine maps) images. B) Example of material decomposition in image domain using dsDECT system. The images obtained at two distinct energies are processed to obtain energy-selective (VMI) and material-selective (iodine maps) images. Source: [29].

This is the concept behind the three-basis-material (or multimaterial) decomposition algorithms 5. Nowadays, the material decomposition and labeling algorithms on the different scanners may use algorithms with graphic vectors.

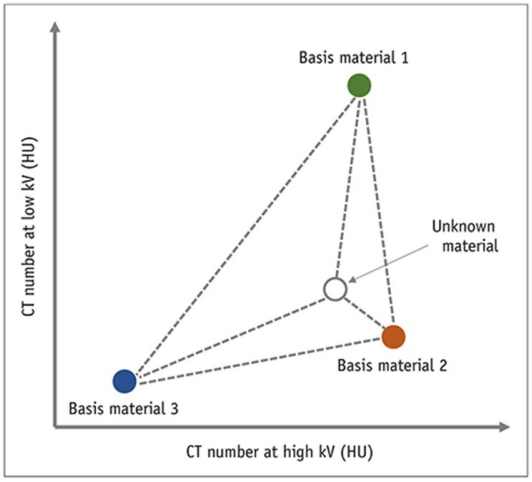

Fig. 5: Illustration of three-material decomposition through a two-dimensional mapping of CT numbers (measured in HU) obtained from a dual-energy scan. In this example, any unknown material falling within the triangle, established by the CT number pairs of the three chosen fundamental materials, can be depicted as a linear combination of these components. Source: [46].

4.3. Material differentiation in BMD assessment for diagnosis of osteoporosis

Two-material decomposition techniques have been widely employed in spectral CT to separate two main materials and provide quantitative information about their composition. In BMD assessment for osteoporosis, the two main materials are often HA and water. There are several studies that have implemented a two-material decomposition algorithm using DLCT scans. In [37], the researchers conducted a two-material decomposition, analyzing HA and water, on spectral images acquired using a DLCT system to quantify BMD in an anthropomorphic spine phantom. The derived BMD values were then compared to DXA results, revealing a high level of accuracy. A distinct approach was employed in [47]. to ascertain BMD in similar anthropomorphic spine phantom and vertebral specimens also using water and HA as basis components. Utilizing the correlation between 50 and 200 keV monoenergetic images and a calibration equation based on a single BDC phantom scan, HU values were translated into BMD values. This method demonstrated exceptional accuracy in phantom data. In vertebral specimens, strong correlations and agreement were established between QCT and spectral-based outcomes. Similarly, in [48], authors utilized a comparable approach to compute BMD values in 33 patients, yielding results comparable to QCT.

However, bone is a complex tissue composed of multiple materials, including red bone marrow (RBM) and marrow adipose tissue (MAT). It has been demonstrated that MAT has a bad effect on BMD quantification leading to

its underestimation [10]. To investigate the extent of the effect MAT on BMD measurements, Sfeir et al. conducted a comparative analysis of single-energy and dual-energy CT (SECT and DECT) performance focused on the trabecular bone compartment of the lumbar spine as well as both the trabecular and cortical compartments of the femoral neck. The DECT method employed a sophisticated three-material decomposition approach, which allowed for the assessment of volume fractions of HA, RBM, and MAT, thus accounting for the presence of marrow fat. Notably, the DECT-derived BMD values were observed to be higher than the corresponding SECT values, with more significant differences noted in the trabecular bone compartments. This variance was notably smaller in the cortical bone compartment, where MAT is not present to the same extent. Furthermore, the underestimation of BMD values by SECT, when compared to DECT, exhibited an incremental trend with decreasing BMD values. The findings from this study shed valuable light on the influence of MAT on BMD measurements and underscore the significance of employing advanced imaging techniques, such as DECT with three-material decomposition, to achieve more precise and comprehensive evaluations of bone health.

Hofmann et al. indicated the potential of a three-material decomposition method to assess BMD in DECT images without the influence of soft tissue and fat, compared to DXA and QCT [14]. They showed that clinical indications align with the DXA gold standard. The workflow they proposed revealed bone degradation effects that are typically imperceptible on standard CT images, potentially leading to inaccuracies in conventional QCT outcomes.

In [15], they successfully implemented a 3-material decomposition algorithm to differentiate acute and chronic thoracolumbar vertebral fractures based on the level of bone marrow edema. This study showed that the detection of bone marrow edema and thus acute vertebral fractures based on three-material decomposition generated from DLCT images was feasible with a substantially higher accuracy compared to conventional CT images.

In [49], Gruenewald et al. assessed BMD for the prediction of osteoporosis-associated fractures using DECT systems and a material decomposition software that differentiates collagen matrix, calcium hydroxyapatite, water, fat marrow, and adipose tissue for each voxel, an algorithm previously proposed by Nickoloff et al. [32]. This allowed the identification of patients at risk to sustain osteoporosis-associated fractures with a sensitivity of 85.45% and a specificity of 89.19%. Additionally, the DECT-derived BMD threshold for the identification of at-risk patients lies above the American College of Radiology (ACR) QCT guidelines for the identification of osteoporosis (93.70 mg/cm^3 vs 80 mg/cm^3). This higher threshold can in part be attributed to the removal of the aforementioned confounding variables as well as the elimination of technical shortcomings that underestimate conventional QCT-based BMD measurements, such as the fat error.

Although most papers focus on non-contrast DECT images, some works have analyzed the effect of intravenously injected contrast for BMD assessment. This is particularly relevant for cancer patients, who suffer from rapid bone loss and undergo contrast-enhanced staging CT scans with DECT mode. Most of these studies [50], [51] have generally concluded that contrast agents have a minor influence, and improved CT imaging remains effective in accurately evaluating trabecular bone mineral content, even when contrast-enhanced scans are compared to unenhanced scans. However, Ma et al. concluded that HA concentration assessed in both enhanced and unenhanced modes might have similar diagnostic efficacy [52].

5. Future directions and discussion

The BMD assessment for osteoporosis diagnosis has two established gold standards: DXA and QCT. However, these two methods exhibit several drawbacks that may render them suboptimal for this specific purpose. Spectral CT (DECT) coupled with material decomposition algorithms have gained attention. Research in this area has shown promising potential to develop a system that surpasses the established clinical standards, offering notably enhanced accuracy.

One of the significant advantages of spectral CT in BMD assessment is the ability to perform phantomless calibration. Traditional BMD assessments often require the use of external phantoms for calibration, which can be time-consuming and may introduce errors. Spectral CT eliminates the need for phantoms, streamlining the process and potentially reducing the risk of inaccuracies associated with phantom-based calibrations. Additionally, spectral CT provides access to the entire energy spectrum of X-rays. In BMD assessment, this allows for a more comprehensive analysis of bone composition, potentially leading to more accurate and detailed information about bone health.

While two-material decomposition techniques have shown substantial progress in BMD assessment, there is potential for further advancement through more sophisticated multi-material decomposition methods. Incorporating additional materials beyond the fundamental constituents, such as red bone marrow and marrow adipose tissue, could enable a more comprehensive and accurate quantification of bone health. By accounting for the complex composition of bone tissue, these advanced approaches could potentially offer enhanced diagnostic accuracy, particularly in cases where the presence of diverse tissue components impacts BMD measurements [10].

Specifically, some considerations could be taken for the research of three-material decomposition algorithms. Firstly, including physiologically relevant materials that have more distinctive attenuation properties could improve BMD assessment given that RBM, water, and MAT have similar attenuation properties [10]. This would signify a less narrow triangle for a three-material decomposition system (see Fig. 5. Additionally, physiological constraints on material concentrations could avoid biologically impossible volume fractions. However, it should be noted that physiological constraints would have to account for the dynamic composition of bone marrow among patients [53]. Another consideration is the site of the image acquisition. The amount of trabecular and cortical

bone impacts the results as trabecular bone shows higher BMD in the spine [19]. Furthermore, multi-material decomposition including more bone components could be investigated. In the study by Gruenewald et al. [49], 5 different materials were quantified using a different algorithm.

The validation and clinical translation of three-material decomposition methods for BMD assessment hold significant promise. Studies like that of Sfeir et al. [10] have begun to shed light on the influence of marrow adipose tissue on BMD measurements. In fact, some studies have found discrepancies with the ACR osteoporosis definition thresholds. Further research in larger patient cohorts and clinical settings could provide valuable insights into the practical impact of these findings. The validation of three-material decomposition algorithms against established gold standards (DXA and QCT) in real-world patient populations would establish the clinical utility and accuracy of these advanced techniques.

Given that DXA and QCT, while established as gold standards, are acknowledged to have inherent limitations, it is imperative to strategize on how to compare a new method to them. Simply seeking a method that performs well in comparison to these standards may not ultimately yield the most optimal solution. One potential approach involves initiating a comprehensive comparative analysis to establish their equivalency. Moreover, employing phantom data may unveil a superior spetral CT coupled with a three-material decomposition (sCT-3MD) method that potentially outperforms the existing standards.

While much of the focus has been on non-contrast DECT images, there is a growing interest in exploring the impact of intravenously injected contrast agents on BMD assessment [50]–[52]. For cancer patients undergoing contrast-enhanced staging CT scans, understanding how contrast agents influence BMD measurements is crucial. Investigating the potential benefits and limitations of using contrast-enhanced DECT for BMD assessment could open new avenues for accurate bone health evaluation, especially in populations with rapid bone turnover.

Integrating machine learning algorithms with spectral CT data holds immense potential for refining BMD assessment. Machine learning models for diagnosing and classifying osteoporosis and detecting fractures from images have shown promising performance. Some studies on this matter are reviewed in [54].

In conclusion, the field of material decomposition in osteoporosis diagnosis is rapidly evolving, with exciting opportunities to enhance the accuracy, specificity, and clinical applicability of BMD assessment using spectral CT techniques. Continued research and innovation in these directions could reshape how osteoporosis is diagnosed, monitored, and managed, ultimately improving patient outcomes and quality of life.

6. Conclusion

In summary, this literature review delves into the advances in the field of three-material decomposition with DECT as a transformative approach for precise BMD assessment for the diagnosis of osteoporosis. By evaluating the existing standards of BMD evaluation, explaining the foundational principles of spectral CT, and discussing the ongoing advancements and limitations within three-material decomposition algorithms, this review offers a detailed and comprehensive overview of the landscape within this evolving field.

We can conclude that spectral CT holds the potential in revolutionizing BMD assessment when compared to current clinical standards such as DXA and QCT. The inherent limitations of DXA and QCT, encompassing susceptibility to overlying structures, body size dependence, radiation exposure, and adipose tissue influence, underscore the urgent need for innovative alternatives.

Spectral CT's distinctive dual-energy techniques, coupled with the refinement of three-material decomposition algorithms, offer a paradigm shift in BMD assessment. By precisely quantifying materials based on distinct attenuation properties at varying energy levels, this technology demonstrates the potential to address the existing challenges. In specific, DLCT, which includes a single detector, appears as a pioneering solution with a lower radiation dose.

Future avenues for research in this field include incorporating additional materials such as MAT and RBM, physiological constraints and considerations related to image acquisition sites. The validation and clinical translation of these algorithms hold substantial promise, as demonstrated by studies highlighting the influence of marrow adipose tissue on BMD measurements. Additionally, investigating the impact of intravenously injected contrast agents on BMD assessment and integrating machine learning algorithms with spectral CT data offer new dimensions for refining BMD assessment.

In conclusion, this literature review underscores the transformative potential of spectral CT and three-material decomposition for advancing BMD assessment in osteoporosis diagnosis. As this field progresses, interdisciplinary collaboration, continued research endeavors, and the translation of innovations into clinical practice will collectively shape a future where accurate, early diagnosis and effective management of osteoporosis are within reach, ultimately enhancing the quality of life for individuals at risk.

References

[1] P.-L. Xiao, A.-Y. Cui, C.-J. Hsu, R. Peng, N. Jiang, X.-H. Xu, Y.-G. Ma, D. Liu, and H.-D. Lu, "Global, regional prevalence, and risk factors of osteoporosis according to the world health organization diagnostic criteria: a systematic review and meta-analysis," *Osteoporosis International*, vol. 33, no. 10, pp. 2137–2153, Jun. 2022. [Online]. Available: https://doi.org/10.1007/s00198-022-06454-3

[2] J. P. Brown, K. Engelke, T. M. Keaveny, A. Chines, R. Chapurlat, A. J. Foldes, X. Nogues, R. Civitelli, T. D. Villiers, F. Massari, C. A. Zerbini, Z. Wang, M. K. Oates, C. Recknor, and C. Libanati, "Romosozumab improves lumbar spine bone mass and bone strength parameters relative to alendronate in postmenopausal women: results from the active-controlled fracture study in postmenopausal women with osteoporosis at high risk (scpARCH)/scp trial," *Journal of Bone and Mineral Research*, vol. 36, no. 11, pp. 2139–2152, Aug. 2021. [Online]. Available: https://doi.org/10.1002/jbmr.4409

[3] J. A. Kanis, O. Johnell, A. Oden, I. Sernbo, I. Redlund-Johnell, A. Dawson, C. D. Laet, and B. Jonsson, "Long-term risk of osteoporotic fracture in malmö," *Osteoporosis International*, vol. 11, no. 8, pp. 669–674, Sep. 2000. [Online]. Available: https://doi.org/10.1007/s001980070064

[4] D. L. Kendler, F. Marin, C. A. F. Zerbini, L. A. Russo, S. L. Greenspan, V. Zikan, A. Bagur, J. Malouf-Sierra, P. Lakatos, A. Fahrleitner-Pammer, E. Lespessailles, S. Minisola, J. J. Body, P. Geusens, R. Möricke, and P. López-Romero, "Effects of teriparatide and risedronate on new fractures in post-menopausal women with severe osteoporosis (VERO): a multicentre, double-blind, double-dummy, randomised controlled trial," *The Lancet*, vol. 391, no. 10117, pp. 230–240, Jan. 2018. [Online]. Available: https://doi.org/10.1016/s0140-6736(17)32137-2

[5] D. Marshall, O. Johnell, and H. Wedel, "Meta-analysis of how well measures of bone mineral density predict occurrence of osteoporotic fractures," *BMJ*, vol. 312, no. 7041, pp. 1254–1259, May 1996. [Online]. Available: https://doi.org/10.1136/bmj.312.7041.1254

[6] K. N. Haseltine, T. Chukir, P. J. Smith, J. T. Jacob, J. P. Bilezikian, and A. Farooki, "Bone mineral density: Clinical relevance and quantitative assessment," *Journal of Nuclear Medicine*, vol. 62, no. 4, pp. 446–454, Dec. 2020. [Online]. Available: https://doi.org/10.2967/jnumed.120.256180

[7] T. M. Link, "Radiology of osteoporosis," *Canadian Association of Radiologists Journal*, vol. 67, no. 1, pp. 28–40, Feb. 2016. [Online]. Available: https://doi.org/10.1016/j.carj.2015.02.002

[8] T. M. Link and G. Kazakia, "Update on imaging-based measurement of bone mineral density and quality," *Current Rheumatology Reports*, vol. 22, no. 5, Apr. 2020. [Online]. Available: https://doi.org/10.1007/s11926-020-00892-w

[9] T. M. Link and T. F. Lang, "Axial QCT: Clinical applications and new developments," *Journal of Clinical Densitometry*, vol. 17, no. 4, pp. 438–448, Oct. 2014. [Online]. Available: https://doi.org/10.1016/j.jocd.2014.04.119

[10] J. G. Sfeir, M. T. Drake, E. J. Atkinson, S. J. Achenbach, J. J. Camp, A. J. Tweed, L. K. McCready, L. Yu, M. C. Adkins, S. Amin, and S. Khosla, "Evaluation of cross-sectional and longitudinal changes in volumetric bone mineral density in postmenopausal women using single- versus dual-energy quantitative computed tomography," *Bone*, vol. 112, pp. 145–152, jul 2018. [Online]. Available: https://doi.org/10.1016%2Fj.bone.2018.04.023

[11] H. K. GENANT and D. BOYD, "Quantitative bone mineral analysis using dual energy computed tomography," *Investigative Radiology*, vol. 12, no. 6, pp. 545–551, Nov. 1977. [Online]. Available: https://doi.org/10.1097/00004424-197711000-00015

[12] C. H. McCollough, S. Leng, L. Yu, and J. G. Fletcher, "Dual- and multi-energy CT: Principles, technical approaches, and clinical applications," *Radiology*, vol. 276, no. 3, pp. 637–653, Sep. 2015. [Online]. Available: https://doi.org/10.1148/radiol.2015142631

[13] S. V. Hedent, K.-H. Su, D. W. Jordan, B. Eck, F. Liang, R. Kessner, J.-W. Kuo, N. Buls, P. Klahr, P. Ros, and R. F. Muzic, "Improving bone mineral density assessment using spectral detector CT," *Journal of Clinical Densitometry*, vol. 22, no. 3, pp. 374–381, jul 2019. [Online]. Available: https://doi.org/10.1016%2Fj.jocd.2018.10.004

[14] P. Hofmann, M. Sedlmair, B. Krauss, J. L. Wichmann, R. W. Bauer, T. G. Flohr, and A. H. Mahnken, "Phantom-less bone mineral density (BMD) measurement using dual energy computed tomography-based 3-material decomposition," in *Medical Imaging 2016: Computer-Aided Diagnosis*, G. D. Tourassi and S. G. Armato, Eds. SPIE, Mar. 2016. [Online]. Available: https://doi.org/10.1117/12.2217413

[15] B. J. Schwaiger, A. S. Gersing, J. Hammel, K. Mei, F. K. Kopp, J. S. Kirschke, E. J. Rummeny, K. Wörtler, T. Baum, and P. B. Noël, "Three-material decomposition with dual-layer spectral CT compared to MRI for the detection of bone marrow edema in patients with acute vertebral fractures," *Skeletal Radiology*, vol. 47, no. 11, pp. 1533–1540, may 2018. [Online]. Available: https://doi.org/10.1007%2Fs00256-018-2981-x

[16] O. of the Surgeon General (US), *Bone Health and Osteoporosis: A Report of the Surgeon General*. Rockville (MD): Office of the Surgeon General (US), 2004. [Online]. Available: https://www.ncbi.nlm.nih.gov/books/NBK45513/

[17] F. Cosman, S. J. de Beur, M. S. LeBoff, E. M. Lewiecki, B. Tanner, S. Randall, and R. Lindsay, "Clinician's guide to prevention and treatment of osteoporosis," *Osteoporosis International*, vol. 25, no. 10, pp. 2359–2381, Aug. 2014. [Online]. Available: https://doi.org/10.1007/s00198-014-2794-2

[18] G. Osterhoff, E. F. Morgan, S. J. Shefelbine, L. Karim, L. M. McNamara, and P. Augat, "Bone mechanical properties and changes with osteoporosis," *Injury*, vol. 47, pp. S11–S20, Jun. 2016. [Online]. Available: https://doi.org/10.1016/s0020-1383(16)47003-8

[19] P. M. Camacho, S. M. Petak, N. Binkley, B. L. Clarke, S. T. Harris, D. L. Hurley, M. Kleerekoper, E. M. Lewiecki, P. D. Miller, H. S. Narula, R. Pessah-Pollack, V. Tangpricha, S. J. Wimalawansa, and N. B. Watts, "American association of clinical endocrinologists and american college of endocrinology clinical practice guidelines for the diagnosis and treatment of postmenopausal osteoporosis — 2016–executive summary," *Endocrine Practice*, vol. 22, no. 9, pp. 1111–1118, 2016. [Online]. Available: https://doi.org/10.4158/ep161435.esgl

[20] S. R. Cummings, M. C. Nevitt, W. S. Browner, K. Stone, K. M. Fox, K. E. Ensrud, J. Cauley, D. Black, and T. M. Vogt, "Risk factors for hip fracture in white women," *New England Journal of Medicine*, vol. 332, no. 12, pp. 767–773, Mar. 1995. [Online]. Available: https://doi.org/10.1056/nejm199503233321202

[21] C. J. Rosen, *The Epidemiology and Pathogenesis of Osteoporosis*. MDText.com, Inc., South Dartmouth (MA), 2000-.

[22] J. A. Kanis, *WHO Study Group. Assessment of fracture risk and its application to screening for postmenopausal osteoporosis: synopsis of a WHO report*. World Health Organization, 1994.

[23] K. Engelke, T. Lang, S. Khosla, L. Qin, P. Zysset, W. D. Leslie, J. A. Shepherd, and J. T. Schousboe, "Clinical use of quantitative computed tomography (QCT) of the hip in the management of osteoporosis in adults: the 2015 ISCD official positions—part i," *Journal of Clinical Densitometry*, vol. 18, no. 3, pp. 338–358, Jul. 2015. [Online]. Available: https://doi.org/10.1016/j.jocd.2015.06.012

[24] J. S. Yu, N. G. Krishna, M. G. Fox, D. G. Blankenbaker, M. A. Frick, S. T. Jawetz, G. Li, C. Reitman, N. Said, J. D. Stensby, N. Subhas, M. Tulchinsky, E. A. Walker, and F. D. Beaman, "ACR appropriateness criteria® osteoporosis and bone mineral density: 2022 update," *Journal of the American College of Radiology*, vol. 19, no. 11, pp. S417–S432, Nov. 2022. [Online]. Available: https://doi.org/10.1016/j.jacr.2022.09.007

[25] J. E. Adams, "Quantitative computed tomography," *European Journal of Radiology*, vol. 71, no. 3, pp. 415–424, Sep. 2009. [Online]. Available: https://doi.org/10.1016/j.ejrad.2009.04.074

[26] "Acr–spr–ssr practice parameter for the performance of musculoskeletal quantitative computed tomography (qct)," *The American College of Radiology*, vol. 1076, no. Resolution 9, p. 6, 2018.

[27] E. Nishimaru, "The fundamental principle in x-ray CT scanner," *Japanese Journal of Radiological Technology*, vol. 71, no. 11, pp. 1123–1131, 2015. [Online]. Available: https://doi.org/10.6009/jjrt.2015_jsrt_71.11.1123

[28] E. C. McCullough, "Photon attenuation in computed tomography," *Medical Physics*, vol. 2, no. 6, pp. 307–320, Nov. 1975. [Online]. Available: https://doi.org/10.1118/1.594199

[29] A. Agostini, A. Borgheresi, A. Mari, C. Floridi, F. Bruno, M. Carotti, N. Schicchi, A. Barile, S. Maggi, and A. Giovagnoni, "Dual-energy CT: theoretical principles and clinical applications," *La radiologia medica*, vol. 124, no. 12, pp. 1281–1295, Dec. 2019. [Online]. Available: https://doi.org/10.1007/s11547-019-01107-8

[30] M. M. GOODSITT, D. I. ROSENTHAL, W. R. REINUS, and J. COUMAS, "Two postprocessing CT techniques for determining the composition of trabecular bone," *Investigative Radiology*, vol. 22, no. 3, pp. 209–215, Mar. 1987. [Online]. Available: https://doi.org/10.1097/00004424-198703000-00005

[31] J. R. Vetter, W. H. Perman, W. A. Kalender, R. B. Mazess, and J. E. Holden, "Evaluation of a prototype dual-energy computed tomographic apparatus. II. determination of vertebral bone mineral content," *Medical Physics*, vol. 13, no. 3, pp. 340–343, May 1986. [Online]. Available: https://doi.org/10.1118/1.595951

[32] E. L. Nickoloff, F. Feldman, and J. V. Atherton, "Bone mineral assessment: new dual-energy CT approach." *Radiology*, vol. 168, no. 1, pp. 223–228, Jul. 1988. [Online]. Available: https://doi.org/10.1148/radiology.168.1.3380964

[33] W. A. Kalender, E. Klotz, and C. Suess, "Vertebral bone mineral analysis: an integrated approach with CT." *Radiology*, vol. 164, no. 2, pp. 419–423, Aug. 1987. [Online]. Available: https://doi.org/10.1148/radiology.164.2.3602380

[34] M. Kirschner, M. Becker, M. Erdt, K. Kafchitsas, M. F. Khan, and S. Wesarg, "Dual-energy CT-based assessment of the trabecular bone in vertebrae," *Methods of Information in Medicine*, vol. 51, no. 05, pp. 398–405, 2012. [Online]. Available: https://doi.org/10.3414/me11-02-0034

[35] J. L. Wichmann, C. Booz, S. Wesarg, K. Kafchitsas, R. W. Bauer, J. M. Kerl, T. Lehnert, T. J. Vogl, and M. F. Khan, "Dual-energy CT–based phantomless in vivo three-dimensional bone mineral density assessment of the lumbar spine," *Radiology*, vol. 271, no. 3, pp. 778–784, Jun. 2014. [Online]. Available: https://doi.org/10.1148/radiol.13131952

[36] J. M. S. Wait, D. Cody, A. K. Jones, J. Rong, V. Baladandayuthapani, and S. C. Kappadath, "Performance evaluation of material decomposition with rapid-kilovoltage-switching dual-energy CT and implications for assessing bone mineral density," *American Journal of Roentgenology*, vol. 204, no. 6, pp. 1234–1241, Jun. 2015. [Online]. Available: https://doi.org/10.2214/ajr.14.13093

[37] R. W. van Hamersvelt, A. M. R. Schilham, K. Engelke, A. M. den Harder, B. de Keizer, H. J. Verhaar, T. Leiner, P. A. de Jong, and M. J. Willemink, "Accuracy of bone mineral density quantification using dual-layer spectral detector CT: a phantom study," *European Radiology*, vol. 27, no. 10, pp. 4351–4359, apr 2017. [Online]. Available: https://doi.org/10.1007%2Fs00330-017-4801-4

[38] F. van Ommen, H. de Jong, J. Dankbaar, E. Bennink, T. Leiner, and A. Schilham, "Dose of CT protocols acquired in clinical routine using a dual-layer detector CT scanner: A preliminary report," *European Journal of Radiology*, vol. 112, pp. 65–71, mar 2019. [Online]. Available: https://doi.org/10.1016%2Fj.ejrad.2019.01.011

[39] R. E. Alvarez and A. Macovski, "Energy-selective reconstructions in x-ray computerised tomography," *Physics in Medicine and Biology*, vol. 21, no. 5, pp. 733–744, Sep. 1976. [Online]. Available: https://doi.org/10.1088/0031-9155/21/5/002

[40] W. A. Kalender, W. Seissler, E. Klotz, and P. Vock, "Spiral volumetric CT with single-breath-hold technique, continuous transport, and continuous scanner rotation." *Radiology*, vol. 176, no. 1, pp. 181–183, Jul. 1990. [Online]. Available: https://doi.org/10.1148/radiology.176.1.2353088

[41] Y. Zhao, Y. Wu, Z. Zuo, and S. Cheng, "CT angiography of the kidney using routine CT and the latest gemstone spectral imaging combination of different noise indexes: image quality and radiation dose," *La radiologia medica*, vol. 122, no. 5, pp. 327–336, feb 2017. [Online]. Available: https://doi.org/10.1007%2Fs11547-017-0739-5

[42] N. Magarelli, V. D. Santis, G. Marziali, A. Menghi, A. Burrofato, L. Pedone, D. D. Prete, R. Iezzi, C. de Waure, M. D'andrea, A. Leone, and C. Colosimo, "Application and advantages of monoenergetic reconstruction images for the reduction of metallic artifacts using dual-energy CT in knee and hip prostheses," *La radiologia medica*, vol. 123, no. 8, pp. 593–600, apr 2018. [Online]. Available: https://doi.org/10.1007%2Fs11547-018-0881-8

[43] K. L. Grant, T. G. Flohr, B. Krauss, M. Sedlmair, C. Thomas, and B. Schmidt, "Assessment of an advanced image-based technique to calculate virtual monoenergetic computed tomographic images from a dual-energy examination to improve contrast-to-noise ratio in examinations using iodinated contrast media," *Investigative Radiology*, vol. 49, no. 9, pp. 586–592, Sep. 2014. [Online]. Available: https://doi.org/10.1097/rli.0000000000000060

[44] R. Offenberg, "Phantomless bone mineral density assessment in patients using dual-energy ct," 2021.

[45] X. Liu, L. Yu, A. N. Primak, and C. H. McCollough, "Quantitative imaging of element composition and mass fraction using dual-energy CT: Three-material decomposition," *Medical Physics*, vol. 36, no. 5, pp. 1602–1609, Apr. 2009. [Online]. Available: https://doi.org/10.1118/1.3097632

[46] A. So and S. Nicolaou, "Spectral computed tomography: Fundamental principles and recent developments," *Korean Journal of Radiology*, vol. 22, no. 1, p. 86, 2021. [Online]. Available: https://doi.org/10.3348%2Fkjr.2020.0144

[47] K. Mei, B. J. Schwaiger, F. K. Kopp, S. Ehn, A. S. Gersing, J. S. Kirschke, D. Muenzel, A. A. Fingerle, E. J. Rummeny, F. Pfeiffer, T. Baum, and P. B. Noël, "Bone mineral density measurements in vertebral specimens and phantoms using dual-layer spectral computed tomography," *Scientific Reports*, vol. 7, no. 1, dec 2017. [Online]. Available: https://doi.org/10.1038%2Fs41598-017-17855-4

[48] F. Roski, J. Hammel, K. Mei, T. Baum, J. S. Kirschke, A. Laugerette, F. K. Kopp, J. Bodden, D. Pfeiffer, F. Pfeiffer, E. J. Rummeny, P. B. Noël, A. S. Gersing, and B. J. Schwaiger, "Bone mineral density measurements derived from dual-layer spectral CT enable opportunistic screening for osteoporosis," *European Radiology*, vol. 29, no. 11, pp. 6355–6363, May 2019. [Online]. Available: https://doi.org/10.1007/s00330-019-06263-z

[49] L. D. Gruenewald, V. Koch, S. S. Martin, I. Yel, K. Eichler, T. Gruber-Rouh, L. Lenga, J. L. Wichmann, L. S. Alizadeh, M. H. Albrecht, C. Mader, N. A. Huizinga, T. D'Angelo, S. Mazziotti, S. Wesarg, T. J. Vogl, and C. Booz, "Diagnostic accuracy of quantitative dual-energy CT-based volumetric bone mineral density assessment for the prediction of osteoporosis-associated fractures," *European Radiology*, vol. 32, no. 5, pp. 3076–3084, oct 2021. [Online]. Available: https://doi.org/10.1007%2Fs00330-021-08323-9

[50] V. Koch, M. H. Albrecht, L. D. Gruenewald, I. Yel, K. Eichler, T. Gruber-Rouh, R. M. Hammerstingl, I. Burck, J. L. Wichmann, L. S. Alizadeh, T. J. Vogl, L. Lenga, S. Wesarg, S. S. Martin, C. Mader, M. Dimitrova, T. D'Angelo, and C. Booz, "Impact of intravenously injected contrast agent on bone mineral density measurement in dual-source dual-energy CT," *Academic Radiology*, vol. 29, no. 6, pp. 880–887, jun 2022. [Online]. Available: https://doi.org/10.1016%2Fj.acra.2021.06.010

[51] S. Jang, P. M. Graffy, T. J. Ziemlewicz, S. J. Lee, R. M. Summers, and P. J. Pickhardt, "Opportunistic osteoporosis screening at routine abdominal and thoracic CT: Normative l1 trabecular attenuation values in more than 20 000 adults," *Radiology*, vol. 291, no. 2, pp. 360–367, may 2019. [Online]. Available: https://doi.org/10.1148%2Fradiol.2019181648

[52] Q. Ma, X. Hou, C. Zhao, Y. Yan, X. Cheng, J. Li, D. Ma, and Z. Yang, "Diagnostic power of vertebral hydroxyapatite concentration measurements in spectral CT for osteoporosis-associated fractures and impact of intravenous contrast administration," *European Radiology*, vol. 33, no. 6, pp. 4016–4023, jan 2023. [Online]. Available: https://doi.org/10.1007%2Fs00330-022-09383-1

[53] B. C. V. Berg, J. Malghem, F. E. Lecouvet, and B. Maldague, "Magnetic resonance imaging of normal bone marrow," *European Radiology*, vol. 8, no. 8, pp. 1327–1334, sep 1998. [Online]. Available: https://doi.org/10.1007%2Fs003300050547

[54] S. H. Kong and C. S. Shin, "Applications of machine learning in bone and mineral research," *Endocrinology and Metabolism*, vol. 36, no. 5, pp. 928–937, oct 2021. [Online]. Available: https://doi.org/10.3803%2Fenm.2021.1111

APPENDIX